Lawrence Berkeley National Laboratory
LBL Publications

Title
Ferromagnetic quantum critical point in CePd2P2 with Pd → Ni substitution

Authors
Lai, Y
Bone, SE
Minasian, S
et al.

Peer reviewed

Ferromagnetic Quantum Critical Point in $CePd_2P_2$ with Pd → Ni Substitution

Y. Lai[1,2], S. E. Bone[3], M. G. Ferrier[3], J. Lezama-Pacheco[4], V. Mocko[3], A. S. Ditter[3,5], S. A. Kozimor[3], G. T. Seidler[5], W. L. Nelson[1,2], Y.-C. Chiu[1,2], K. Huang[1], W. Potter[6], D. Graf[1], T. E. Albrecht-Schmitt[6], R. E. Baumbach[1,2,*]

[1]*National High Magnetic Field Laboratory, Florida State University, Tallahassee, FL 32310, USA*
[2]*Department of Physics, Florida State University, Tallahassee, FL 32306, USA*
[3]*Los Alamos National Laboratory, Los Alamos, NM 87544*
[4]*Stanford University, Stanford, CA 94305*
[5]*University of Washington, Seattle WA 98195 and*
[6]*Department of Chemistry and Biochemistry, Florida State University,Tallahassee, FL 32306, USA*
(Dated: January 11, 2018)

An investigation of the structural, thermodynamic, and electronic transport properties of the isoelectronic chemical substitution series $Ce(Pd_{1-x}Ni_x)_2P_2$ is reported, where a ferromagnetic quantum critical point is uncovered in the temperature - concentration $(T - x)$ phase diagram. This behavior results from the simultaneous contraction of the unit cell volume, which tunes the relative strengths of the Kondo and RKKY interactions, and the introduction of disorder through alloying. Consistent with this picture, x-ray absorption spectroscopy measurements reveal a transformation from $CePd_2P_2$ having a purely trivalent cerium f-state to $CeNi_2P_2$ having a small amount of tetravalent character. In the quantum critical region near $x_{cr} \approx 0.7$, there is a breakdown of Fermi liquid behavior, signaling the influence of quantum fluctuations. Measurements of clean $CePd_2P_2$ furthermore show that applied pressure has a similar initial effect to alloying on the ferromagnetic order. From these results, $CePd_2P_2$ emerges as a keystone system to test theories such as the Belitz-Kirkpatrick-Vojta model for ferromagnetic quantum criticality, where distinct behaviors are expected in the dirty and clean limits.

PACS numbers: PACS

I. INTRODUCTION

Heavy fermion f-electron intermetallics continue to attract interest because many of them exhibit complex phase diagrams with diverse phenomena including nematic electronic states, charge and spin instabilities, and unconventional superconductivity. [1–5] In many cases this is related to a competition between the RKKY and Kondo interactions, which mediate magnetism and compensate localized spins, respectively. [6–10] The fine balance between these interactions can cause a magnetic ordering temperature to be continuously suppressed towards zero temperature at a quantum critical point (QCP). As this occurs novel behaviors often emerge including the breakdown of Fermi liquid behavior and the emergence of superconductivity. [4, 11] This has led to a viewpoint that quantum fluctuations of an order parameter are key for producing novel phenomena, and this phenomenology even spans diverse families of materials that are distinct from f-electron intermetallics: e.g., cuprate and iron-based superconductors, [12, 13] organic superconductors, [14] charge density wave systems, [15] and others.

There nonetheless remain many open questions, including how the specific type of magnetism being suppressed influences a quantum critical region. The earliest theories of quantum phase transitions focused on ferromagnetism, [16] and the seminal work of Hertz and Millis predicted that a ferromagnetic phase transition would remain continuous to zero temperature. [17, 18] More recent work by Belitz-Kirkpatrick-Vojta (BKV) demonstrates instead that for clean materials in two and three dimensions a zero temperature transition from ferromagnetism to paramagnetism is discontinuous. [5] This precludes the occurrence of diverging fluctuations of the magnetic order parameter, which may interfere with phenomena such as unconventional superconductivity as seen near some antiferromagnetic QCPs. The BKV theory also predicts that there is a tricritical point that separates a high temperature line of second order phase transitions from a low temperature line of first order phase transitions, where the application of a magnetic field produces wing-like second order phase boundaries that intercept zero temperature. In disordered systems the tricritical point is pushed below zero temperature and the second order phase boundary extends to zero temperature. This has spurred interest in ferromagnetic quantum criticality in disordered metals, where an intriguing possibility is that they might host anomalous metallic states and even unconventional superconductivity. [5, 19] It is noteworthy that while there are several uranium-based ferromagnetic superconductors [20–23], there are no cerium-based analogues despite the electronic similarities beween the associated $5f$ and $4f$ states.

$CePd_2P_2$ was recently reported to be a correlated electron ferromagnet crystallizing in the well-known $ThCr_2Si_2$-type structure [24, 25], while its isoelectronic volume compressed analogue $CeNi_2P_2$ exhibits a nonmagnetic ground state. [26, 27] This suggests that the Pd → Ni alloy series could host a ferromagnetic quan-

tum critical point. We synthesized single crystal specimens of $Ce(Pd_{1-x}Ni_x)_2P_2$ for $0 < x < 1$, where there is a monotonic unit cell contraction that applies a chemical pressure. X-ray diffraction and magnetic susceptibility measurements show that the cerium ions remain nearly trivalent at elevated temperatures across the entire series, while x-ray absorption spectroscopy for $CePd_2P_2$ and $CeNi_2P_2$ reveal trivalent and trivalent with a small fraction of tetravalent f-electron character, respectively. Features associated with the ferromagnetic ordering are evident in magnetic susceptibility, heat capacity, and electrical resistivity, where the ordering temperature is continuously suppressed up to $x_{cr} \approx 0.7$. In the critical region there is chemical disorder which allows the phase transition to remain second order, even as it approaches zero temperature. This results in a putative ferromagnetic QCP, around which there are indications for a breakdown of Fermi liquid behavior: (1) the heat capacity divided by temperature C/T diverges logarithmically with decreasing T and (2) the electrical resistivity ρ follows a sub-quadratic temperature dependence. We furthermore find that for clean $CePd_2P_2$, applied pressure initially suppresses the ferromagnetism in a manner similar to that of Pd $\rightarrow$ Ni substitution. Therefore, this system offers the opportunity to study behavior at a disordered ferromagnetic quantum critical point and eventually to compare to the ordered analogue, as is needed to test the BKV theory and to ultimately design new quantum critical point materials.

II. EXPERIMENTAL METHODS

Single crystals of $Ce(Pd_{1-x}Ni_x)_2P_2$ were grown from elements with purities$> 99.9\%$ in a molten flux of Pd, Ni and P. The reaction ampoules were prepared by loading the elements in the ratio Ce:Pd:Ni:P ; 1:11(1-x):11x:8 into a 2 mL alumina crucible for each of the nominal Ni concentrations. The crucibles were sealed under vacuum in quartz ampoules and heated to $300\,°C$ at a rate of $50\,°C$/hour, held at $300\,°C$ for 6 hours, heated to $500\,°C$ at a rate of $50\,°C$/hour, held at $500\,°C$ for 6 hours, heated to $1180\,°C$ at a rate of $50\,°C$/hour, kept at $1180\,°C$ for 3 hours, and then cooled at a rate of $2\,°C$/hour to $1000\,°C$. At this temperature, the remaining flux was separated from the crystals by centrifuging. Single-crystal platelets with typical dimensions of several millimeters on a side and several millimeters in thickness were collected.

The crystal structure and chemical composition were verified by powder x-ray-diffraction (XRD) and energy dispersive spectrometer (EDS) analysis. EDS results are shown in Fig. 1a, where the measured concentration x_{act} is compared to the nominal concentration x_{nom}. Throughout the rest of the manuscript we use x_{act} unless otherwise specified. Magnetization $M(T, H)$ measurements were carried out for single crystals at temperatures $T = 1.8 - 300$ K under an applied magnetic field of $H = 5$ kOe for H applied both parallel ($\parallel$) and perpen-

dicular ($\perp$) to the c axis using a Quantum Design VSM Magnetic Property Measurement System. Electrical resistivity ρ measurements for temperatures $T = 0.5 - 300$ K and magnetic fields $H = 0 - 9$ T were performed in a four-wire configuration and the heat capacity C was measured for $T = 0.39 - 20$ K using a Quantum Design Physical Property Measurement System. For select concentrations, $\rho(T)$ was measured for $T \gtrsim 100$ mK using a QD adiabatic demagnetization refrigerator. $\rho(T)$ measurements under applied pressure were performed using a piston cylinder pressure cell with Daphne 7474 oil as the pressure transmitting medium. The pressure is determined by the shift in ruby flourescence peaks and are the values determined below $T = 10$ K. These measurements were performed at the National High Magnetic Field Laboratory DC field User facility using standard He3 cryostats.

Samples were analyzed using Ce L_3-edge X-ray absorption spectroscopy (XAS) at the Stanford Synchrotron Radiation Lightsource (SSRL) on beam line 11-2. Single crystals of the compounds were ground and diluted with boron nitride. Samples were painted onto 0.5 mil Kapton tape, attached to an aluminum sample plate and loaded into a liquid helium cryostat. The cryostat was separated from the beam pipe by a continuously flowing helium flight path. A single energy was selected using a liquid-N2-cooled double-crystal monochromator utilizing Si(220) ($\phi = 0$) crystals. The crystals were detuned by 70% at 6100 eV to remove higher order harmonics. The monochromator was calibrated based on the energy of the first inflection point of a chromium calibration foil (5989.0 eV). All spectra were measured in fluorescence mode using a Lytle detector equipped with a Ti filter (3 absorption lengths) at two different temperatures, 85 and 10 K, using a liquid He-cooled cryostat. No Soller slits were used. A Cr-calibration foil was placed downstream of the sample so that the monochromator calibration could be monitored during every sample scan.

Using the Athena11 software package, the spectral background was eliminated by (1st) fitting a line to the pre-edge region (5673 to 5703 eV) and (2nd) subtracting the line from the experimental data. The spectra were normalized by fitting a second-order polynomial to the post-edge region of the spectrum (5753 to 5798 eV) and setting the edge jump at E_0 (5723 eV) to an intensity of 1.0, thereby normalizing intensities for each spectrum to a single Ce atom. A deconvoluted model for the Ce L_3-edge XAS data was obtained using a modified version of EDG- FIT [28] in IGOR 6.0. Using this least-squares algorithm between 5705 and 5741 eV, the main absorption peak (5725) and any possible post-edge features were fit with a minimum number of pseudo-Voight functions (50:50 Lorentzian:Gaussian). An additional function was employed that consisted of a 1:1 ratio of arctangent and error function contributions to model the absorption threshold. No constraints were used in modeling the data. The areas under the pre-edge peaks (hereafter defined as the intensity) were equal to the FWHM

x peak height.

III. RESULTS

Powder X-ray diffraction measurements show that the $ThCr_2Si_2$-type structure persists across entire the Pd $\rightarrow$ Ni substitution series, while the tetragonal lattice constants (a and c) and the unit cell volume (V) decrease with increasing x (Fig. 1). These trends are consistent with Vegard's law, where the lattice contraction is due to the smaller size of Ni by comparison to Pd and suggest that the room temperature Ce valence remains nearly trivalent with increasing x. The volume contraction results in a chemical pressure which is estimated to be near $P_{ch} = 13.6$ GPa for $x = 0.955$. This value is calculated using the Birch-Murnaghan equation $P_{ch} = B_0 \Delta V(x)/V(0)$, where the value of the bulk modulus for $CeCu_2Si_2$ ($B_0 = 110$ GPa) is used.[29]
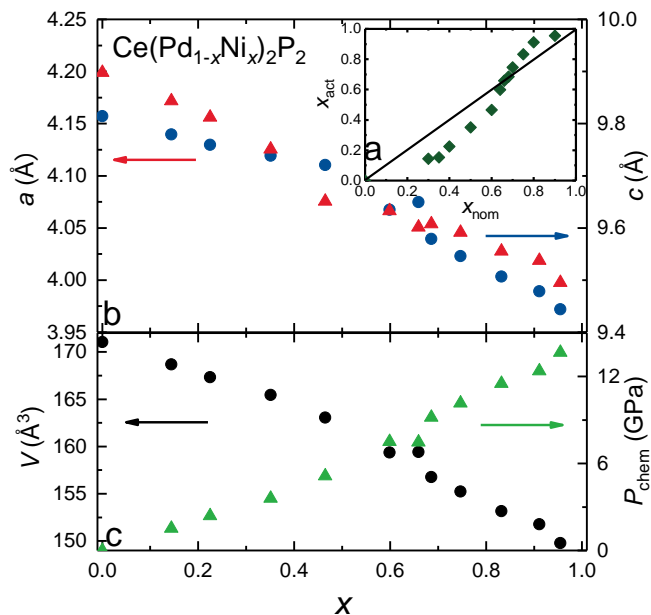

FIG. 1. (a) Comparison between the measured phosphorous concentration x_{act} and the nominal concentration x_{nom}, where x_{act} was determined using energy dispersive spectrometer analysis. Throughout the rest of the manuscript we use $x_{act} = x$ unless otherwise specified. (b) The lattice constants, $a(x)$ (left axis) and $c(x)$ (right axis). (c) the unit cell volume $V(x)$ (left axis) and chemical pressure P_{ch}(right axis), calculated using the Birch-Murnaghan equation as described in the text with the bulk modulus $B_0 = 110$ GPa.

The magnetic susceptibility $\chi = M/H$ vs temperature and magnetization M vs H for $H \parallel c$ data are shown in Fig. 2, where the high T behavior provides insight into the x-evolution of the f-electron state, magnetocrystalline anisotropy, and strength of the Kondo hybridization. $\chi(T)$ for $CePd_2P_2$ follows a Curie Weiss (CW) temperature dependence for $150\ K < T < 300\ K$ (Fig. 2b)

with large anisotropy between the $H \parallel c$ and in-plane directions where the (001)-direction is the easy axis. [24, 25] The CW behavior persists across the entire substitution series and fits to the data reveal effective magnetic moments $\mu_{eff} \approx 2.5 - 2.6\ \mu_B/Ce$, as expected for trivalent cerium. The magnetic anisotropy decreases by roughly a factor of 10 to approach $\chi_\perp/\chi_\parallel \approx 20$ near $x \approx 0.35$, after which it recovers to nearly the $x = 0$ value at $x \approx 0.6$ and finally decreases to become isotropic at $x = 1$ (Fig. 2). The Curie-Weiss temperature θ is positive at $x = 0$, consistent with a ferromagnetic exchange interaction. It subsequently changes sign from positive to negative near $x \approx 0.66$ (Fig. 2c), after which its magnitude grows rapidly. A large and negative θ is a common feature in Ce-based materials with strong hybridization between the f- and conduction electrons and indicates an enhanced Kondo interaction at large x.
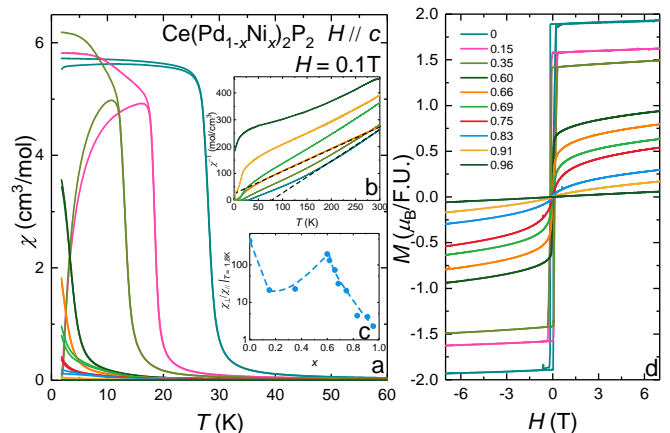

FIG. 2. (a) Magnetic susceptibility $\chi = M/H$ vs temperature T for $H = 0.1$ T applied parallel $\parallel$ to the c-axis for $Ce(Pd_{1-x}Ni_x)_2P_2$. (b) The inverse of Magnetic susceptibility $\chi^{-1}(T)$ for representative curves with $H \parallel c$. The dotted lines are Curie-Weiss fits to the data for $150\ K < T < 300$ K. (c) The magnetic anisotropy $\chi_\perp/\chi_\parallel$ vs x at $T = 2$ K. (d) Magnetization field dependence for different x-concentrations measured at 1.8K.

To further evaluate the effect of Pd $\rightarrow$ Ni substitution on the Ce f-electron state, Ce L_3-edge X-ray absorption spectra (XAS) were obtained from single crystals of $CeNi_2P_2$ and $CePd_2P_2$, the end members of the series. Typically, Ce^{III} provides a single absorption peak at ca. 5723-5725 eV, whereas Ce^{IV} exhibits a "double-white line" feature with maxima at ca. 5724-5728 and 5736-5739 eV. As shown in Fig. 3, the Ce L_3-edge spectrum from $CePd_2P_2$ was typical of Ce^{III}, containing a single pronounced absorption peak with a maximum at 5725.2 eV (FWHM = 6.60 eV). Although substituting Ni for Pd had essentially no impact on the main absorption peak energy (maximum = 5725.1 eV), subtle spectral changes emerged; most notably, the main absorption peak broadened by 1.24 eV (FWHM = 7.84 eV) and a

minor post-edge feature emerged near 5735 eV. Additionally, spectra obtained from $CeNi_2P_2$ and $CePd_2P_2$ were unchanged as a function of temperature between 85 and 10 K.

To characterize the origin of these changes, the Ce L_3-edge XAS spectra were modeled using a least-squares algorithm between 5705 and 5741 eV. Although the entire fitted region for $CePd_2P_2$ was easily modeled by the combination of a single peak at 5725.2 eV and a step-function at 5724.4 eV, an analogous model for $CeNi_2P_2$ did not adequately represent the data. In particular, there was substantial misfit associated with the post-edge feature that was absent in the $CePd_2P_2$ spectrum. Hence, three peaks and a step-function were needed to model the $CeNi_2P_2$ spectrum. The main absorption peak was at 5725.1 eV, the step function at 5723.0 eV, and two post-edge peaks were fit at 5732.6 and 5735.7 eV. We believe it is of no coincidence that the highest-energy post-edge peak (at 5735.7 eV) occurred at a similar energy to the higher energy peak of the "double-white line" feature typically observed for Ce^{IV} (between 5736 and 5739 eV). [30–39] Hence, we interpreted the data as indicating $CeNi_2P_2$ contained a mixture of Ce^{III} and Ce^{IV}. Comparison of the intensities (FWHM x peak height) of the main absorption peak (intensity = 8.8) with the small post-edge peaks (intensities = 0.2 and 0.4) suggested that $CeNi_2P_2$ contained on the order of 7(1)% Ce.

Returning to the bulk signatures of the magnetism, the $x = 0$ ferromagnetic ordering appears in $\chi(T)$ as a sharp increase at $T_C = 28.5$ K, which is straightforward to define as the peak in $\partial\chi/\partial T$ (not shown). For $T \leq T_C$, $M(H)$ for $x = 0$ rapidly saturates towards $M_{sat} = 1.93$ μ_B. We track the evolution of the ferromagnetic order with x using these quantities, where it is evident that T_C decreases linearly for $x \lesssim 0.66$, after which it occurs at temperatures lower than those reached in this measurement or has been completely suppressed. The persistence of the ferromagnetism is also seen in the $M(H)$ curves, which retain their step-like shapes even as M_{sat} is smoothly suppressed (Fig. 2d). For $x \gtrsim 0.66$, the magnitudes of $\chi(T)$ and $M(H)$ continue to decrease and become similar to that of paramagnetic $CeNi_2P_2$ as x approaches 1.[27]

The heat capacity C divided by T vs. T data are shown in Fig. 4a, which further expose the ordered state and underlying electronic behavior. The $x = 0$ ferromagnetism appears as a lambda-like feature near $T_C = 28.5$ K, consistent with a second order phase transition. With increasing x, T_C moves to lower temperatures and up to $x \approx 0.35$ the shape of phase transition is preserved but its overall size grows. This indicates that even as T_C is suppressed the associated entropy is conserved. Between $0.35 < x \lesssim 0.69$, the ferromagnetic feature broadens and is superimposed on an increasing background. The broadening of the phase transition is attributed to chemical/structural disorder which is maximal near the middle of the substitution series. As T_C approaches zero near $x_{cr} \approx 0.7$, C/T diverges nearly continuously down
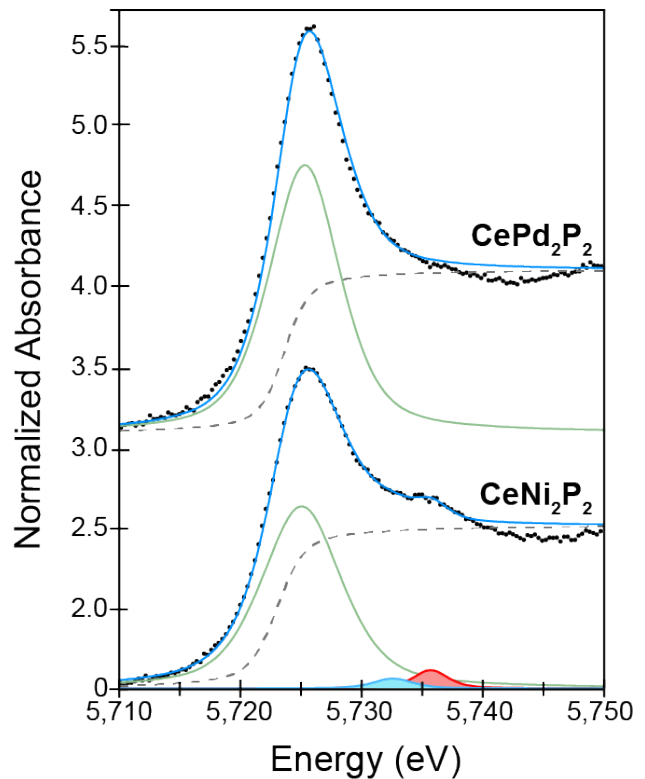

FIG. 3. The experimental data (dots) and the curve fitted model (blue trace) for the Ce L_3-edge X-ray absorption spectra of $CePd_2P_2$ (top) and $CeNi_2P_2$ (bottom). The pre-edge pseudo-Voigt functions (green, blue, and red traces) used to generate the model and the step function (grey dashed lines) are shown.

to 0.5 K. This is a common feature of 'non-Fermi-liquid' behavior near a quantum critical point in correlated f-electron materials and and is associated with quantum fluctuation of the magnetic order parameter. [1–5] For larger x the divergence weakens and finally tends to saturate at low temperature for $x = 0.96$ in a manner that is similar to $CeNi_2P_2$, indicating the recovery of the paramagnetic Fermi liquid state.

The $4f$ contribution to the entropy S_{4f} vs. T is shown in Fig. 4b. S_{4f} was calculated by subtracting C/T for the nonmagnetic analogue $La(Pd_{1-x}Ni_x)_2P_2$ from that of $Ce(Pd_{1-x}Ni_x)_2P_2$ and subsequently integrating from 0.5 K. The nonmagnetic lattice term was approximated by summing the heat capacities of $LaPd_2P_2$ and $LaNi_2P_2$ in the ratios $(1-x):x$. While this approach slightly underestimates the total $4f$ entropy and only approximates the lattice contribution to the heat capacity, it provides a consistent way to assess the evolution of S_{4f} with x. S_{4f} reaches $0.88R\ln2$ at T_C for $x = 0$. This is reduced from the full entropy of a a doublet ground state and is due to some Kondo screening of the f-moment by the conduction electrons. [24, 25] In the x-region where the phase transition remains sharp ($0 \leq x \lesssim 0.35$), S_{4f} con-
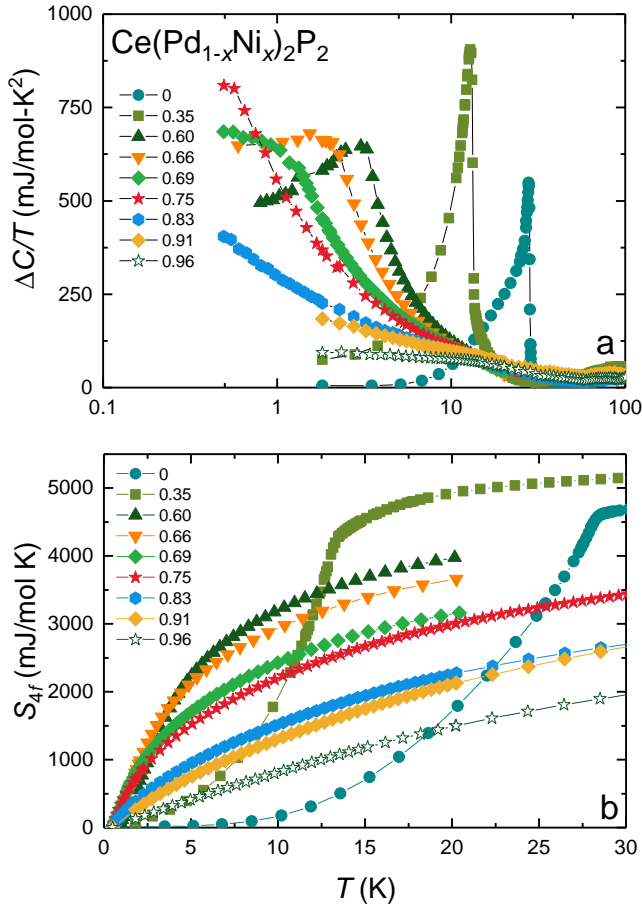
FIG. 4. (a) The heat capacity C divided by temperature T vs T following the phonon background subtraction described in the text for select concentrations of Ce(Pd$_{1-x}$Ni$_x$)$_2$P$_2$. (b) $4f$ entropy S_{4f} vs x. S_{4f} is obtained from the heat capacity data as described in the text.

FIG. 5. (a) and (b) The electrical resistivity normalized to the room temperature value ρ/ρ_{300K} vs. temperature T for Ce(Pd$_{1-x}$Ni$_x$)$_2$P$_2$ at values $x = 0 - 1$. (c) Power law fits to the low temperature electrical resistivity for selected concentration of Ce(Pd$_{1-x}$Ni$_x$)$_2$P$_2$ near x_{cr}. (d) $\rho/\rho_{300K}(T)$ collected under applied pressure $P \lesssim 19$ kbar for CePd$_2$P$_2$.

sistently recovers to similar values at T_C, suggesting that the strength of the hybridization changes little over this range. For specimens with larger concentrations that still show ferromagnetism but have broadened phase transitions ($0.35 \lesssim x \lesssim 0.69$), the entropy recovered at T_C grows smaller with increasing x, which reveals strengthening hybridization. For concentrations in the no order region ($0.83 \lesssim x \lesssim 1$) S_{4f} is significantly reduced from that seen at lower x and increases smoothly with increasing T in a manner consistent with there being strong Kondo hybridization between the f- and conduction electrons.[6, 7]

The temperature dependences of the electrical resistivity normalized to the room temperature value ρ/ρ_{300K} vs. T for the entire substitution series are shown in Fig. 5. The behavior for $x = 0$ is consistent with earlier results, where the resistivity decreases with decreasing T and evolves through a kink near $T_C = 28.5$ K that further reduces the electronic scattering due to the removal of
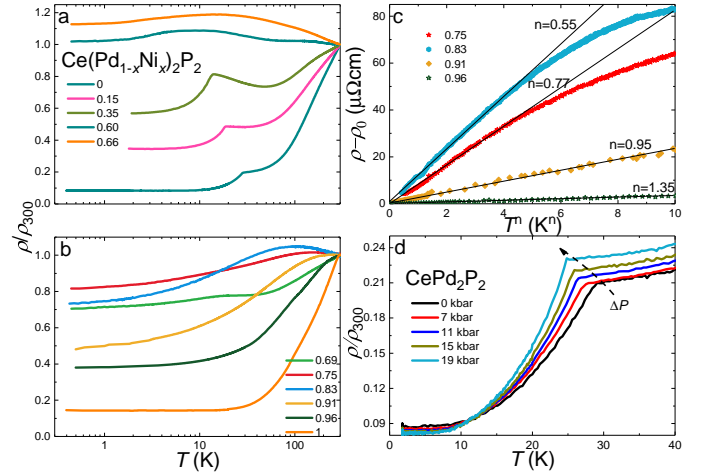
magnetic fluctuations. [24] Here, the residual resistivity ratio $RRR = \rho/\rho_{300K} \approx 12$. For $0 \leq x \lesssim 0.35$ RRR decreases due to increasing disorder, but the reduction in ρ/ρ_{300K} at T_C remains sharp. This is consistent with heat capacity measurements showing that the growing disorder does not strongly influence the ordering on this x-range. In addition, over this x-range the phase transition is preceded by a growing upturn in ρ/ρ_{300K} which indicates strengthening magnetic scattering of conduction electrons prior to the phase transition. For larger x the phase transition broadens due to increasing disorder and continues to be suppressed until it is no longer visible near $x_{cr} \approx 0.7$.

In the region near x_{cr}, power law behavior of the form $\rho(T) = \rho_0 + AT^n$ is seen, where the best fits are obtained by plotting $\rho - \rho_0$ versus T^n and adjusting the value of ρ_0 to maximize the range of linear behavior (Fig. 6c). From this analysis, we find pronounced deviations from T^2 Fermi liquid behavior. Similar "non-Fermi-liquid" behavior is observed for a wide variety of other cerium based materials where a second order phase transition is suppressed to zero temperature [1–4], providing further evidence that there is a quantum critical point near x_{cr} in this alloy series. In the large x region where ferromagnetism is absent, the low temperature resistivity decreases as the disorder scattering weakens. Over this range, the Fermi liquid behavior of the pure Ni parent compound is gradually recovered.

Finally, in order to further examine the tuning mechanisms that control the ordered state in CePd$_2$P$_2$, we performed measurements of the electrical resistivity under hydrostatic pressure (Fig. 5d). We find that the ferromagnetic phase transition is monotonically suppressed

with increasing pressure at a rate of 2.4 K/GPa, and from this we estimate that an applied pressure of 12 GPa would be needed to fully suppress the ferromagnetism to zero temperature in the parent compound. In order to directly compare this result to what is seen for Pd → Ni substitution, we convert the applied pressure to change in unit cell volume and then associate this value with a Ni concentration. Results for a typical bulk modulus $B_0 \approx$ 110 GPa (similar to what is observed for CeCu$_2$Si$_2$ [29]) are shown as open stars in Fig. 6a, where the slope of T_C is weaker than that seen in the substitution series.

IV. DISCUSSION

Fig. 6 shows the $T - x$ phase diagram and the evolution of several quantities vs. x. T_C is suppressed linearly with x, and approaches zero near $x_{cr} \approx 0.7$. For $x = 0$ we also plot results from measurements under applied pressure, where chemical and applied pressure both continuously suppress T_C. If we assume $B_0 = 220$ GPa (closed stars) then both chemical and applied pressure suppress T_C at the same rate. A more realistic value of $B_0 = 110$ GPa (open stars) results in a more gradual suppression of T_C. Regardless of which B_0 is chosen, it is clear that the main tuning parameter that controls T_C is the unit cell volume, which likely changes the relative strengths of the Kondo and RKKY interactions in a Doniach-like scenario.[6] Importantly, for the chemical substitution series the phase transition remains second order across the entire range ferromagnetic x-regime. This is understood by considering that strong disorder is seen in the intermediate substitution region: e.g., as a broadening of the phase transition in heat capacity and as growing residual resistivity that peaks near $x \approx 0.6$. This provides the conditions that are expected from the BKV theory for a ferromagnetic quantum critical point near $x_{cr} \approx 0.7$. In contrast, we expect that for clean CePd$_2$P$_2$ the phase transition will become first order near the extrapolated P_{cr}.

Further insight is gained from the temperature dependences of the heat capacity and electrical transport. Between $0 < x \lesssim 0.35$, the low T heat capacity is dominated by a sharp lambda-like feature at T_C. Here, the electronic contribution to the heat capacity is enhanced by comparison to the non-f-electron analogue, indicating a modest Kondo hybridization strength. [24, 25] For $x \leq x_{cr}$ the $4f$ entropy at T_C is conserved up to $x \approx 0.35$, after which it decreases with increasing x. This is consistent with a strengthening hybridization between the f-and conduction electron states which compensates the f-moment, as is also suggested by the weakening values of μ_{sat} upon approaching x_{cr}. As the quantum critical region is approached with increasing x, C/T becomes a combination of a broadened lambda-like peak at T_C and a steadily increasing background which follows a nearly logarithmic temperature dependence. The logarithmic term is maximal near x_{cr}, after which it subsides with increasing
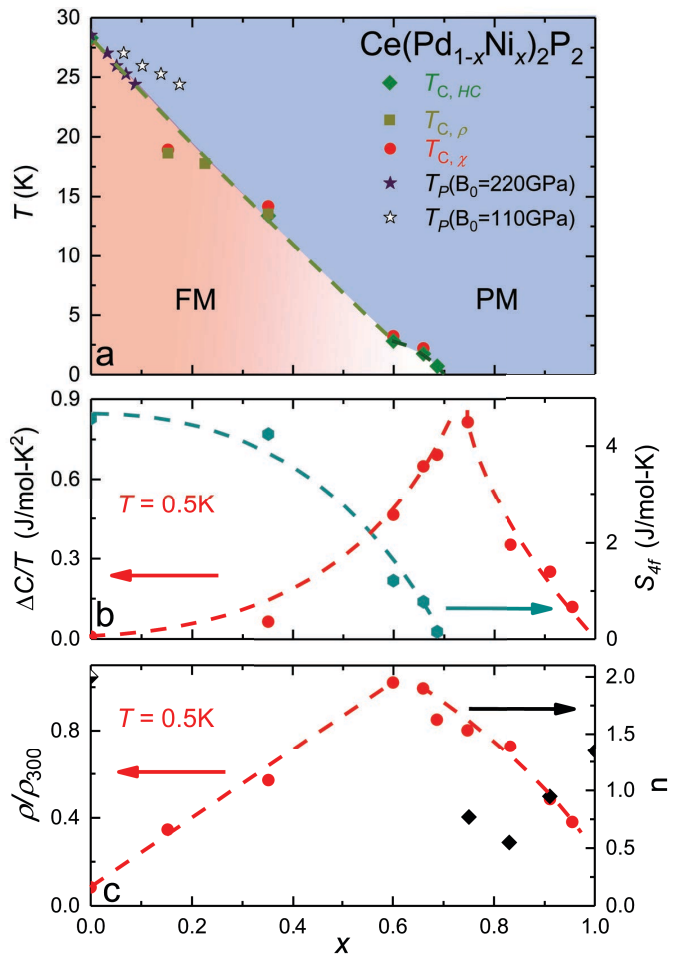

FIG. 6. (a) Temperature T vs. concentration x phase diagram for Ce(Pd$_{1-x}$Ni$_x$)$_2$P$_2$ for $x = 0 - 1$ constructed from magnetic susceptibility $\chi = M/H$, electrical resistivity ρ and heat capacity C data. The red region indicates ferromagnetic (FM) order and the color gradient from red to pink represents increasing disorder. The blue region shows the $T - x$ range with paramagnetism (PM). Also shown is the ferromagnetic phase boundary that was observed for CePd$_2$P$_2$ under applied pressure. The Birch-Murnaghan equation of state was used to convert from pressure to unit cell volume, and then to the corresponding x. The solid and open stars are for $B_0 = 110$ and 220 GPa, respectively. (b) Left axis: The value of the background subtracted heat capacity divided by temperature $\Delta C/T$ at $T = 0.5$ K. Right axis: The $4f$ contribution to the entropy at T_C vs x. (c) Left axis: Electrical resistivity normalized to the room temperature value ρ/ρ_{300K} at $T = 0.5$ K vs x. Right axis: Power-law exponent n resulting from fits to low T $\rho(T)$ vs x.

x (Fig. 6b). This is similar to what is seen in other Ce-based quantum critical materials with the ThCr$_2$Si$_2$-type structure (e.g., the low temperature values of C/T at x_{cr} for the structurally similar CeCu$_2$Si$_{2-x}$Ge$_x$ is 0.9 J/mol K^2 [40]). Evidence for non-Fermi-liquid behavior in the critical region is also seen in the sub-quadratic power-

law temperature dependence of the electrical resistivity, which evolves non-monotonically with x (Fig. 6c).

V. CONCLUSIONS

These results reveal that $Ce(Pd_{1-x}Ni_x)_2P_2$ is a prototypical example of a cerium-based intermetallic with a disordered ferromagnetic QCP and accompanying breakdown of Fermi liquid behavior. Importantly, we also find that for $CePd_2P_2$ a pressure of $P_c \approx 12$ GPa would likely be sufficient to access the tricritical point and first order quantum phase transition that is expected in the clean limit. It will be useful to compare the electronic states that appear near x_{cr} and P_{cr} to test expectations from BKV theory. Further comparison to more conventional antiferromagnetic QCPs is also of interest, where an important question is whether unconventional superconductivity can occur near a disordered ferromagnetic QCP. A significant obstacle in this system may be the disorder, but note that for some disordered ferromagnetic and antiferromagnetic superconductors superconductivity persists even under such conditions.[41, 42]

VI. ACKNOWLEDGEMENTS

[1] G. R. Stewart, *Reviews of Modern Physics* **73**, 797-855 (2001).
[2] H. v. Löhneysen, A. Rosch, M. Vojta, and P. Wölfle, *Reviews of Modern Physics* **79**, 1015-1075 (2007).
[3] P. Gegenwart, Q. Si, and F. Steglich, *Nature Physics* **4**, 186-197 (2008).
[4] C. Pfleiderer, *Reviews of Modern Physics* **81**, 1551-1624 (2009).
[5] M. Brando, D. Belitz, F. M. Grosche, T. R. Kirkpatrick, *Reviews of Modern Physics* **88**, 025006 (2016).
[6] S. Doniach, *Physica B + C* **91**, 231-234 (1977).
[7] J. Kondo, *progress of Theoretical Physics* **32**, 37-49 (1964).
[8] M. A. Ruderman, C. Kittel, *Physical Review* **96**, 99-102 (1954).
[9] T. Kasuya, *progress of Theoretical Physics* **16**, 45-57 (1956).
[10] K. Yosida, *Physical Review* **106**, 893-898 (1957).
[11] J. D. Thompson, Z. Fisk, *Journal of the Physical Society of Japan* **81**, 011002 (2012).
[12] B. J. Ramshaw, S. E. Sebastian, R. D. McDonald, James Day, B. S. Tan, Z. Zhu, J. B. Betts, R. Liang, D. A. Bonn, W. N. Hardy, N. Harrison, *Science* **348**, 317-320 (2015).
[13] J. P. Paglione, R. L. Greene, *Nature Physics* **6**, 645-658 (2010).
[14] N. Doiron-Leyraud, P. Auban-Senzier, S. R. de Cotret, C. Bourbonnais, D. Jérome, K. Bechgaard, L. Taillefer, *Physical Review B* **80**, 214531 (2009).
[15] T. Gruner, D. Jang, Z. Huesges, R. Cardoso-Gil, G. H. Fecher, M. M. Koza, O. Stockert, A. P. Mackenzie, M. Brando, and C. Geibel, *Nature Physics* **13**, 967-972 (2017).
[16] E. C. Stoner, *Proceedings of the Royal Society A* **165**, 372-414 (1938).
[17] J. A. Hertz, *Physical Review B* **14**, 1165-1184 (1976).
[18] A. J. Millis, *Physical Review B* **48**, 7183-7196 (1993).
[19] K. Huang, J. J. Hamlin, R. E. Baumbach, M. Janoschek, N. Kanchanavatee, D. A. Zocco, F. Ronning, M. B. Maple, *Physical Review B* **87**, 054513 (2013).
[20] S. S. Saxena, P. Agarwal, K. Ahilan, F. M. Grosche, R. K. W. Haselwimmer, M. J. Steiner, E. Pugh, I. R. Walker, S. R. Julian, P. Monthoux, G. G. Lonzarich, A. Huxley, I. Sheikin, D. Braithwaite, J. Flouquet, *Nature* **406**, 587-592 (2000).
[21] N. T. Huy, A. Gasparini, D. E. de Nijs, Y. Huang, J. C. P. Klaasse, T. Gortenmulder, A. de Visser, A. Hamann, T. Görlach, H. v. Löhneysen, *Physical Review Letters* **99**, 067006 (2007).
[22] D. Aoki, A. Huxley, E. Ressouche, D. Braithwaite, J. Flouquet, J.-P. Brison, E. Lhotel, C. Paulsen, *Nature* **413**, 613-616 (2001).

[23] T. Akazawa, H. Hidaka, H. Kotegawa, T. C. Kobayashi, T. Fujiwara, E. Yamamoto, Y. Haga, R. Settai, Y. Ōnuki, *Physica B: Condensed Matter* **359-361**, 1138-1140 (2005).

[24] V. H. Tran, Z. Bukowski, *Journal of Physics: Condensed Matter* **26**, 255602 (2014).

[25] Y. Ikeda, H. Yoshizawa, S. Konishi, S. Araki, T. C. Kobayashi, T. Yokoo, S. Ito, *Journal of Physics: Conference Series* **592**, 012013 (2015).

[26] W. Jeitschko and M. Reehuis, *Journal of Physics and Chemistry of Solids* **48**, 667-673 (1987).

[27] J. Chen, Z. Wang, Y. Li, C. Feng, J. Dai, G. Cao, Z.-A. Xu, Q. Si, arxiv:1704.02487(2017).

[28] G. N. George, EDG-FIT.

[29] I. L. Spain, F. Steglich, U. Rauchschwalbe, H. D. Hochheimer, Physica B **449**, 139-140 (1986).

[30] A. Bianconi, A. Marcelli, H. Dexpert, R. Karnatak, A. Kotani, T. Jo, J. Petiau, *Physical Review B* **35**, 806-812 (1987).

[31] G. Kaindl, G. Schmiester, E. V. Sampathkumaran, P. Wachter, *Physical Review B* **38**, 10174(R) (1988).

[32] T. K. Sham, R. A. Gordon, S. M. Heald, *Physical Review B* **72**, 035113 (2005).

[33] M. D. Walter, C. H. Booth, W. W. Lukens, R. A. Andersen, *Organometallics* **28**, 698-707 (2009).

[34] M. W. Löble, J. M. Keith, A. B. Altman, S. C. E. Stieber, E. R. Batista, K. S. Boland, S. D. Conradson, D. L. Clark, J. Lezama Pacheco, S. A. Kozimor, R. L. Martin, S. G. Minasian, A. C. Olson, B. L. Scott, D. K. Shuh, T. Tyliszczak, M. P. Wilkerson, R. A. Zehnder, *Journal of the American Chemical Society* **137**, 2506-2523 (2015).

[35] J. A. Bogart, A. J. Lewis, M. A. Boreen, H. B. Lee, S. A. Medling, P. J. Carroll, C. H. Booth, E. J. Schelter, *Inorganic Chemistry* **54**, 2830-2837 (2015).

[36] S. K. Cary, M. G. Ferrier, R. E. Baumbach, M. A. Silver, J. Lezama Pacheco, S. A. Kozimor, H. S. La Pierre, B. W. Stein, A. A. Arico, D. L. Gray, T. E. Albrecht-Schmitt, *Inorganic Chemistry* **55**, 4373-4380 (2016).

[37] A. N. Kravtsova, A. A. Guda, J. Goettlicher, A. V. Soldatov, V. K. Taroev, A. A. Kashaev, L. F. Suvorova, V. L. Tauson, *Journal of Physics: Conference Series* **712**, 012096 (2016).

[38] M. R. Antonio, R. J. Ellis, S. L. Estes, M. K. Bera, *Physical Chemistry Chemical Physics* **19**, 21304-21316 (2017).

[39] L. M. Toscani, A. F. Craievich, M. C.A. Fantini, D. G. Lamas, S. A. Larrondo, *The Journal of Physical Chemistry C* **120**, 24165-24175 (2016)

[40] G. Knebel, C. Eggert, D. Engelmann, R. Viana, A. Krimmel, M. Dressel, and A. Loidl, *Physical Review B* **53**, 11586 (1996).

[41] A. Gasparini, Y. K. Huang, N. T. Huy, J. C. P. Klaasse, T. Naka, E. Slooten, A. de Visser, *Journal of Low Temperature Physics* **161**, 134-147 (2010).

[42] H. Q. Yuan, F. M. Grosche, M. Deppe, G. Sparn, C. Geibel, and F. Steglich, *Physical Review Letters* **96**, 047008 (2006).